Seventh International Congress on Advances in Civil Engineering, October 11-13, 2006
Yildiz Technical University, Istanbul, Turkey

Understanding and Assessment of Debonding Failures in FRP-Concrete Systems

Oral Büyüköztürk, Tzu-Yang Yu
Massachusetts Institute of Technology, Department of Civil and Environmental Engineering, Cambridge, U.S.A.

Abstract

Failures in FRP-strengthened reinforced concrete (RC) members may occur by flexural failures of critical sections or by debonding of FRP plate from the RC beams. Debonding in the FRP/adhesive/concrete interface region may cause a significant decrease in member capacity leading to a premature failure of the system. There is a need for improved knowledge of the debonding processes under mechanical and environmental effects. In addition, it is essential to develop appropriate nondestructive evaluation techniques for the inspection of these systems for safe application of strengthening concrete structures using FRP composites. In the first part of this paper, various debonding modes are discussed and modeling techniques are introduced. Effects of moisture and temperature on debonding of these multi-layered systems are described. The second part of this paper introduces a nondestructive inspection technique for FRP-strengthened concrete structures using far-field airborne radar. In this development, emphasis is placed on inspection of debonding in GFRP-wrapped concrete cylinders, but the method would also be applicable to beams and slabs with bonded GFRP composites. Radar measurements on physical laboratory specimens with structural damages are described. The measurement results are provided and numerical simulation and imaging studies are summarized.

Keywords: FRP, concrete, debonding, durability, inspection, radar.

Introduction

The use of fiber reinforced polymer (FRP) bonded to deteriorated, deficient, and damaged reinforced concrete structures has gained popularity in Europe, Japan, and North America. High-strength FRPs offer great potential for lightweight, cost-effective retrofitting of concrete infrastructure through external bonding to concrete members to increase their stiffness and load carrying capacity. Theoretical gains in flexural strength using this method can be significant; however, researchers have also observed new

types of failures that can limit these gains. These failures are often brittle, involving delamination of the FRP, debonding of concrete layers, and shear collapse, and can occur at load levels lower than the predicted theoretical strength of the retrofit system. Among these failure modes are fracture of concrete along the planes in the vicinity of FRP-adhesive interfaces, debonding or peeling of the FRP from the concrete surface due to the mechanical and environmental effects, and epoxy decohesion; yet, little is known about the fracture processes and characteristics of these mechanisms. Gradual debonding of the FRP composite under service load conditions may result in premature failures of the retrofitted system. Thus, there is a need for improved knowledge of the delamination and peeling failure processes under various effects; and, durability of FRP-strengthened concrete systems must be characterized. In addition, for inspection of debonding, appropriate nondestructive evaluation (NDE) techniques must be developed. This is essential for safe application of such strengthening of concrete structures using FRP composites.

This paper consists of two parts. The first part discusses the various mechanisms of debonding in FRP/adhesive/concrete systems. Approaches to the modeling of debonding are introduced. Moisture effect is identified as a critical factor in debonding failures of such systems from experimental results. Effects of moisture on debonding are quantified from initial tests. The second part of the paper focuses on the nondestructive method for the inspection of FRP/adhesive/concrete debonding. Particularly, a new NDE technique based on the far-field radar measurements developed by the authors is described. In this development, emphasis is placed on inspection of debonding in GFRP-wrapped concrete cylinders. However, the method would also be applicable to other structural elements such as beams and slabs strengthened by GFRP composites. Radar measurements on physical laboratory specimens with structural damages are described. Radar measurement results are provided and numerical simulation and imaging studies are summarized.

Debonding Failures

Debonding Problems

Failures in FRP-strengthened reinforced concrete (RC) members may occur by flexural failures of critical sections, such as FRP rupture and crushing of compressive concrete, or by debonding of FRP plate from the RC beams. The latter type occurs with a loss in the composite action between the bonded FRP and the RC member. Debonding in FRP strengthened RC members occurs in regions of high stress concentrations, which are often associated with material discontinuities and with the presence of cracks. Propagation path of debonding initiated from stress concentrations depends on the elastic and strength properties of the repair and substrate materials as well as their interface fracture properties. The term “debonding failure” is often used to describe a significant decrease in member capacity due to initiation or propagation of a major crack in the vicinity of the interface region. Theoretically, debonding can occur within a constituent element, or at the interfaces of the materials that form the strengthening system, favoring a propagation path with the least amount of energy. Crack propagation within a material is generally preferred over interface debonding in the design of structural joints. However, interface debonding is often encountered in cases of poor surface preparation. A majority of the debonding failures has been reported to take place

in the concrete substrate. Nevertheless, depending on the geometric and material properties and mechanical and environmental effects to which the interface region is subjected to, other debonding mechanisms can also occur. Experimental results have shown that FRP debonding is a highly complex phenomenon that can involve failure propagation within the concrete substrate, within the adhesive, within the FRP laminate, and the interfaces of these layers (Büyüköztürk et al, 1999a; Smith and Teng, 2001; Büyüköztürk et al, 2003; Büyüköztürk et al, 2004; Gunes, 2004; Au, 2006; Au and Büyüköztürk, 2006a).

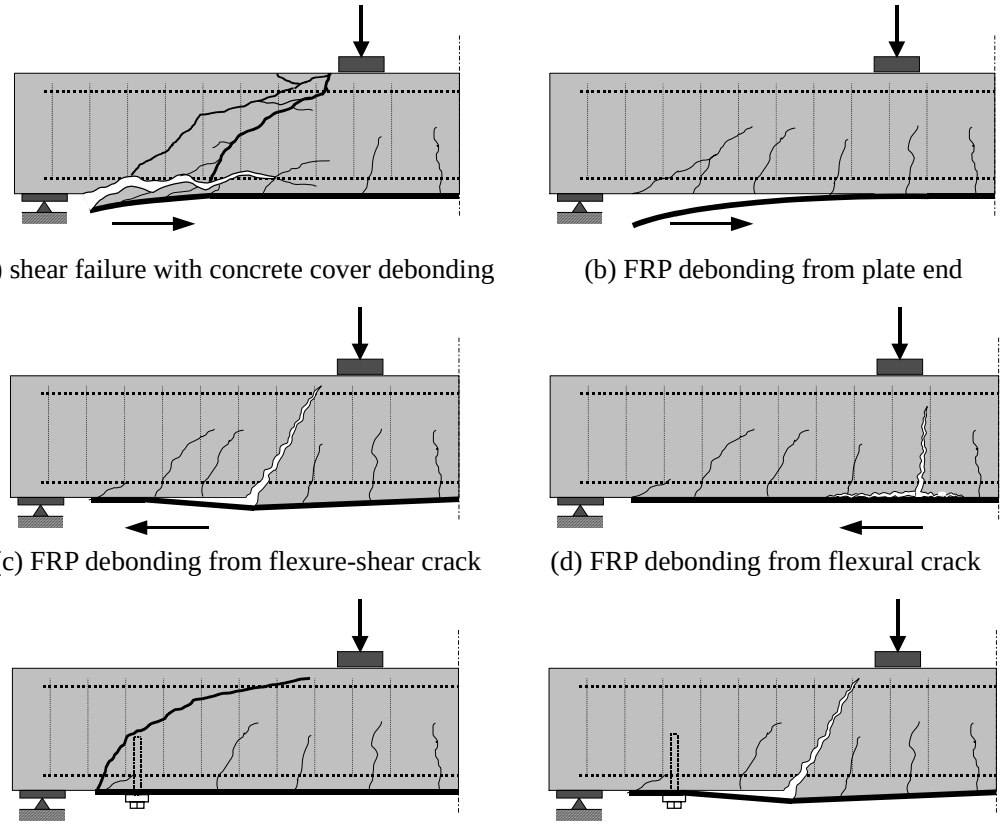

(a) shear failure with concrete cover debonding (b) FRP debonding from plate end

(c) FRP debonding from flexure-shear crack (d) FRP debonding from flexural crack

(e) plate end shear failure (f) shear failure and debonding

Figure 1 Debonding failure mechanisms (Gunes, 2004).

Fundamental debonding mechanisms that may result in premature failure of FRP strengthened beams with and without plate end anchorage are shown in Figure 1. They are (a) shear failure with concrete cover debonding, (b) FRP debonding from plate end, (c) FRP debonding from flexure-shear crack, (d) FRP debonding from flexural crack, (e) plate end shear failure, and (f) shear failure and debonding. The mechanism of shear failure with concrete cover debonding (Fig. 1(a)) is usually associated with high interfacial stresses, low concrete strength, and/or with extensive shear cracking. If the concrete strength and the shear capacity of the beam are sufficiently high, potential debonding failure is most likely to take place through FRP debonding (Fig. 1(b)), which initiates at the plate ends and propagates towards the center of the beam. Depending on the material properties, FRP debonding may occur within the FRP plate, at the concrete-FRP interface, or a few millimeters within the concrete. If the shear span of the strengthened beam is sufficiently long to enable proper bond development, or the plate ends are anchored by

some means, debonding may initiate at flexure-shear cracks and propagate towards the ends of the beam (Fig. 1(c)). If the shear capacity of the beam is sufficiently high, debonding may also initiate from flexural cracks (Fig. 1(d)). However, this failure mechanism is very rare, especially in four-point bending tests. Propagation of debonding within the constant moment region does not change the stress distribution within the strengthened system, thus, a conceptual interpretation suggests that debonding propagation within the constant moment region is energetically not justified. It is possible that high stress concentrations around flexural cracks may promote debonding (Leung, 2001), however, such stress concentrations diminish rapidly with propagation of debonding, resulting in a limited debonded area.

Shear failures in flexurally strengthened beams with insufficient shear capacities become more distinct when plate end anchorage methods are employed to prevent debonding failures. Plate end anchor bolts are able to prevent debonding from plate ends, in which case the beam may fail through shear outside the plated length (Fig. 1(e)). The loading levels at shear failure are approximately 60-65 percent of the theoretical shear capacities of the beams. An alternative failure mode with beams strengthened in flexure using prestressed and non-prestressed FRP plates with or without plate end anchor bolts was also observed (Fig. 1(f)). This failure mode was due to a large flexure-shear crack within the shear span of the beam, leading to debonding of the external FRP reinforcement and shear failure of the beam.

Modeling of Debonding

Characterization and modeling of debonding in structural members strengthened with externally bonded reinforcement has long been a popular field of interdisciplinary research due to critical importance of debonding failures in bonded joints. Research efforts have been concentrated on understanding the causes and mechanisms of debonding failures through theoretical, numerical, and experimental approaches. Research studies in this area can generally be classified as strength and fracture approaches. Additionally, a number of researchers have proposed relatively simple semi-empirical and empirical models for convenient implementation in design calculations. These approaches are briefly introduced in the following sections.

Strength Approach

Prediction of debonding failures through strength approach involves calculation of the interfacial or bond stress distribution in FRP-strengthened RC members. Elastic properties of materials are used in determining stresses which are compared with the ultimate strength of the materials to predict the mechanism and load level of debonding failures. Strength approach predicts bond stress distributions in plate beams assuming all materials are linearly elastic, although concrete cracking is considered. This approach gives approximate solution when constant shear and normal stresses in the adhesive layer are also assumed (Roberts, 1989; Roberts and Haji-Kazemi, 1989). Solutions by higher-order analysis can be obtained when varying shear and normal stresses are used in the analysis (Ziraba et al, 1994; Varastehpour and Hamelin, 1997; El-Mihilmy and Tedesco, 2001). Failure criteria for predicting debonding based on the maximum shear and normal stresses, biaxial stresses in concrete, and a Mohr-Coulomb

type stress state are proposed (Roberts and Haji-Kazemi, 1989; Ziraba et al, 1994; Quantrill et al, 1996; Varastehpour and Hamelin, 1997; Malek et al, 1998; El-Mihilmy and Tedesco, 2001). A review of debonding failure modes and modeling of debonding as a basis for practical design of FRP strengthening of RC beams is given in Teng (2006).

Semi-empirical and empirical models

The use of simplified relations on a phenomenological basis to predict debonding failures leads to the development of semi-empirical and empirical models. Since no stress or fracture mechanics analysis is involved in these models, their validity holds only for a group of RC structures with certain strengthening and loading conditions (Oehlers, 1992; Ahmad et al, 2001; Colotti and Spadea, 2001; Smith and Teng, 2002). General application of semi-empirical and empirical models needs the support of sufficient amount of experimental data covering all possible strengthening configurations.

Fracture approach

From the fracture mechanics point of view, debonding is essentially a crack propagation promoted by local stress intensities. Elastic and fracture properties of materials are utilized in developing predictive models by fracture approach. Finite element method (FEM) and linear elastic fracture mechanics (LEFM) approach have been used for modeling and calculating interface fracture energy, along with experimental measurements (Hamoush and Ahmad, 1990; Karbhari and Engineer, 1996; Fukuzawa et al, 1997; Büyüköztürk et al, 1999b; Rabinovitch and Frostig, 2001; Lau et al, 2001; Leung, 2001).

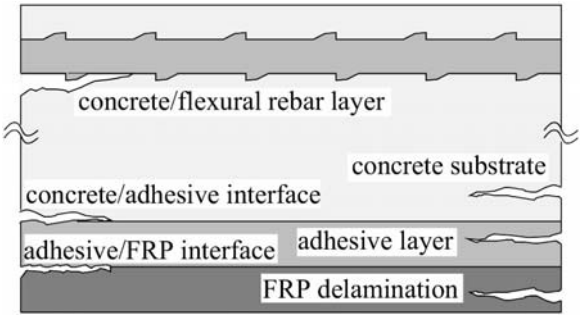

Figure 2 Types of debonding in FRP strengthened RC members.

The term “debonding” is generally used to describe a variety of failures in the vicinity of the bond interface where a parent crack propagates parallel to the plane of the interface. For FRP bonded concrete, three materials (FRP, adhesive, and concrete) and two interfaces (FRP/adhesive and adhesive/concrete) are involved. In theory, five distinct failure modes are possible. They are (a) FRP delamination, (b) FRP/adhesive separation, (c) adhesion decohesion, (d) adhesive/concrete separation, and (e) concrete substrate fracture. Figure 2 illustrates each of the possible five debonding scenarios. These five failure modes can broadly be classified as two classes of failure: (1) material decohesion and (2) interface fracture. Failure (a), (c), and (e) are considered material decohesion while failure (b) and (d) are considered interface fracture. These different

failure modes are partly attributed to the fact that the adhesive bond line thickness in such retrofitted systems is relatively large, usually in the order of the thickness of the FRP laminate, which is in the mm range.

Recently, Au and Büyüköztürk (2006b) proposed a tri-layer interface facture model to facilitate the quantification of various debonding scenarios in FRP/adhesive/concrete plated systems. Central to this development is the use of interface toughness as the quantification parameter of the FRP/epoxy/concrete systems, which is considered a bond property, to analyze, compare, and correlate physical observations. With the explicit material and geometric descriptions and the general boundary conditions, the tri-layer interface facture model provides a basis for parametric study and modeling of debonding in different specimen configurations.

Moisture Effect on Debonding

FRP composites are known for their resistance to environmental conditions. However, durability of the FRP-strengthened RC system remains a major concern in rehabilitation applications. Environmental parameters that have been tested usually include the following: extreme temperature cycles, continuous frozen state, continuous fresh water conditioning, continuous saltwater conditioning, wet/dry cycles using saltwater, freeze-thaw cycles, and UV exposure under sustained load, from which wet/dry cycling is more often tested. Behavior of FRP-strengthened RC systems subjected to freeze-thaw, wet-dry, and temperature variation cycles or various aqueous solutions prior to loading have been studied by researchers and varying degrees of strength degradation have been observed (Chajes et al, 1995; Toutanji and Gomez, 1997; Karbhari and Zhao, 1998; Green et al, 2000; Hamilton, 2000; Di Tommaso et al, 2001).

The influence of moisture on the adhesive is believed to play a critical role in the debonding failure of FRP/adhesive/concrete systems. Absorption of moisture in adhesives depresses the glass transition temperature, for both ambient cured adhesives and for heat-cured adhesives. This could be a particular concern to the FRP-retrofitted RC structures using ambient cured adhesives whose glass transition temperature is typically in the range of 40°C – 60°C, within the vicinity of upper bound service temperature. With further depression by moisture, the adhesive materials may behave viscoelastically under normal service conditions, reducing the stress transfer over time, and upsetting the purpose of the retrofit exercise. The plasticization effect of moisture, on the other hand, enhances the fracture toughness of adhesives due to greater plastic deformation and enhanced crack-tip blunting mechanisms (Kinloch, 1982). Cohesive strength may, however, be reduced (Antoon and Koenig, 1980; Hutchinson, 1986) to sufficiently offset the increased toughness.

Experimental study of debonding in FRP/adhesive/concrete systems in peel and shear failures affected by moisture and temperature has been reported by Au and Büyüköztürk (2006a). Figure 3 (a) illustrates actual debonding configuration and Figure 3 (b) the peel and shear fracture modes, along with CFRP-concrete specimens. Figures 4 and 5 show the peel and shear debonding failure modes in different moisture (dry and wet) and temperature (23°C and 50°C) conditions.

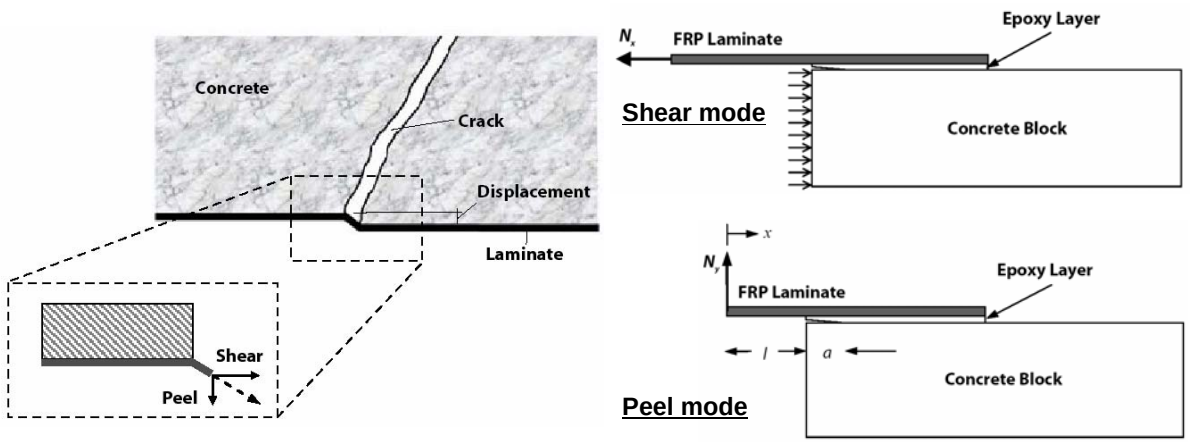

(a) Actual debonding configuration (b) limiting bound fracture models

Figure 3 Actual debonding configuration and limiting bound fracture models (Au and Büyüköztürk, 2006a).

For specimens failed in peel debonding modes (Figure 4), it is found that all dry specimens failed by concrete delamination, suggesting a material decohesion mode. The precrack, which was introduced at the adhesive/concrete interface, kinked into the concrete substrate near the adhesive/concrete interface on the first crack advance, and continued to facture parallel to the interface until complete peel off. A thin layer of concrete was found adhered to the debonded strip, which consisted of an intact adhesive layer. On the other hand, wet specimens exhibited a distinct adhesive/concrete interface separation.

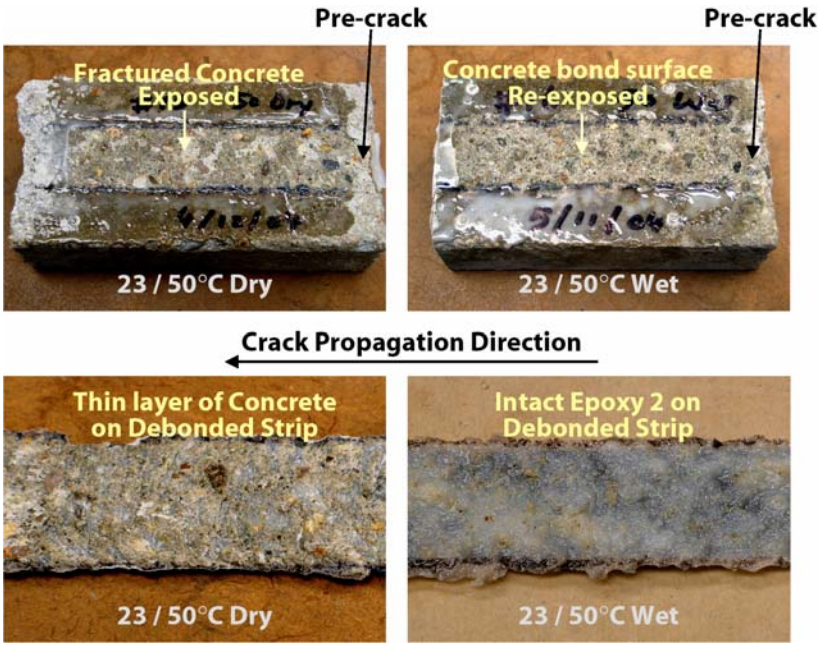

Figure 4 Peel debonding modes (Au and Büyüköztürk, 2006a).

For specimens failed in shear debonding modes (Figure 5), debonding occurred with a rapid propagation, as opposed to the crack-and-halt progressive manner. Concrete

delamination was observed for dry specimens. Wet specimens exhibited an adhesive/concrete interface separation as in the peel debonding.

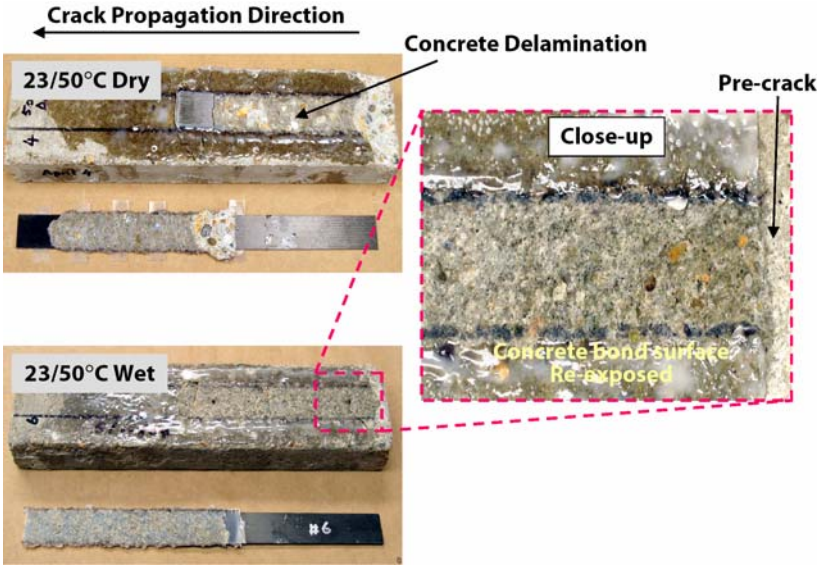

Figure 5 Shear debonding modes (Au and Büyüköztürk, 2006a).

Average values of peel fracture toughness and their trends show a significant drop when specimens were moisture conditioned for 2 weeks or more, as shown in Figure 6(a). Since adhesive/concrete interface separation took place for wet specimens and the fracture toughness values were sharply reduced, it is suggested that the constituent material limits were not fully utilized as concrete did not fracture and adhesive did not craze. Average values of shear fracture toughness and their trends were reported in Figure 6(b). It is found that accelerated moisture diffusion, with the aid of elevated temperature, has resulted in a degradation of more than 50% of the original (dry) shear fracture toughness in as short as 8 weeks, although the reduction slowed down and became more asymptotic starting at the 4-week interval. A similar but slower degradation trend is also observed for moisture conditioning without elevated temperature.

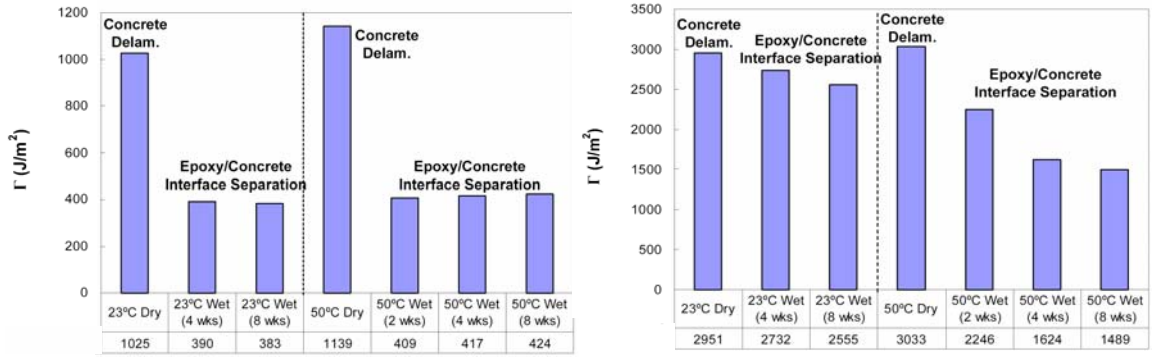

(a) Peel fracture toughness (b) Shear fracture toughness

Figure 6 Fracture toughness variations (Au and Büyüköztürk, 2006a).

These preliminary results show that durability may be an important issue in FRP/adhesive/concrete systems. Variations in environmental conditions such as moisture and temperature may weaken the bond strength at the interface and trigger debonding failures in such systems. Further research is needed to better understand the effects of moisture and other environmental effects with respect to debonding in these composite systems.

In view of the importance of debonding in assessing the integrity of FRP/concrete systems, early detection of such debonding failures in FRP/adhesive/concrete systems by means of nondestructive techniques is necessary. Nondestructive testing techniques are needed especially because with the FRP layer bonded onto the concrete surface, the interface region beneath the FRP layer is not visible and a destructive testing would endanger the integrity of the structural system. Inspection techniques for debonding using NDE (nondestructive evaluation) techniques are introduced in the following part of this paper; emphasis is placed on the far-field airborne radar NDE technique developed by the authors.

Inspection for Debonding using NDE Techniques

In this part of the paper, we describe a far-field airborne radar NDE technique for the nondestructive testing of GFRP-wrapped concrete systems. First, existing NDE techniques for FRP-strengthened concrete systems are reviewed. Introduction to the far-field airborne radar NDE is then followed. Simulation of structural damages in GFRP-wrapped concrete cylinders, physical radar measurements and measurement schemes, radar measurement results, and numerical simulation results are discussed.

Review of NDE Techniques for Debonding

Since debonding failures are brittle in nature, there is little or no precursor before the failure reaches its final stage. Therefore, inspection techniques that can detect debonding at the early stage of failure are needed for FRP-strengthened RC structures. Traditional maintenance inspection for RC structures relies on the surface condition of concrete. With the wrapping of FRP composites such information is no longer available. To “see through” the FRP layer various NDE techniques have been developed, including acoustic emission (Tanigawa et al, 1997; Mirmiran and Philip, 2000; Chen and He, 2001; Swit, 2004), ultrasonic (Popovics and Rose, 1994; Bastianini et al, 2001; Mirmiran and Wei, 2001; Berriman et al, 2006), infrared thermography (Clark et al, 2003; Starnes et al, 2003; Hag-Elasfi et al, 2004), X-ray (Owen, 1998; Daigle et al, 2005), and radar/microwave techniques (Büyüköztürk, 1998; Li and Liu, 2001; Feng et al, 2002; Büyüköztürk et al, 2003; Akuthota et al, 2004).

Among existing NDE techniques, the radar/microwave NDE is less vulnerable to environmental disturbance and is capable of conducting distant inspection. These characteristics make radar NDE advantageous to practical applications in civil engineering. Most of the studies apply contact or near-field measurement schemes using waveguides or specially-made antenna arrays (Li and Liu, 2001; Feng et al, 2002; Akuthota et al, 2004). The use of contact and near-field measurements for NDE may not

be practical for site applications. Furthermore, the spherical/circular wave encountered in near-field measurements is much more complicated than the plane wave in far-field measurements for the purpose of signal processing and image reconstruction. In view of these constraints, the far-field measurement scheme is favored for its potential applicability in detecting the debonding failures of FRP-strengthened RC systems.

Far-field Radar NDE Technique

Far-field radar NDE involves the generation and transmission of electromagnetic (EM) impulse/wave using horn antenna(s) and the design of data collection mode (relative movement between antenna and structure). EM waves are transmitted and received by horn antennas in designed operation mode for data processing/imaging purposes. For structures made of non-metallic materials, EM waves will propagate through the structure with/without attenuation and simultaneously produce reflected waves. For lossy (conductive) materials, transmitted waves are small in amplitude and reflected waves are usually used. Difference between incident and reflected EM waves can related to the dielectric properties of materials (electrical permittivity, electrical conductivity, and magnetic permeability) and the geometric configuration of the structure. In other words, materials with different dielectric properties are identified by the change between incident and reflected EM waves, and interpreted by the variation in reflection coefficient. Therefore, voids, delaminations, rebars, and material characteristics can be detected. Debonding in FRP-strengthened RC systems is thus logically simulated by the insertion of air voids between FRP and concrete, and can be inspected based on the discussed principle.

It is known that EM waves cannot penetrate metallic media and attenuate in conductive media. Therefore, optimization between penetration depths and detection capability for civil structures could be a challenge. For example, in geotechnical applications (e.g., ground penetrating radar), low frequency EM waves (0.05~1GHz) are usually adopted to achieve better exploration depth but with sacrificed detectability (resolution). When operating in free space and with proper development of wideband, multi-frequency capability and tomographic imaging techniques, along with measurement of dielectric properties of the subject materials, radar NDE can be a powerful tool in assessing structural members that consist of hybrid materials, such as GFRP-strengthened concrete structures. To better utilize radar NDE for FRP-strengthened RC systems, their EM response needs to be systematically studied.

The far-field airborne radar (FAR) NDE technique for the inspection of GFRP-strengthened concrete structures was developed at the Massachusetts Institute of Technology (MIT) in collaboration with the MIT Lincoln Laboratory. The proposed radar NDE technique mainly consists of an airborne horn antenna, a signal generator, a signal modulator, and an analyzer. The horn antenna is placed beyond the far-field distance from the target structure. The radar measurements are collected in inverse (or circular) synthetic aperture radar (ISAR) mode; in other words, the reflected signals are received at different angles with respect to the structure. Image reconstruction utilizing the filtered backprojection algorithm is then carried out using the reflected EM wave as a basis for condition assessment.

Possible structural damages that can occur to actual GFRP-retrofitted RC columns are schematically illustrated in Figure 7(a). Structural damages including concrete cracking in the interface region and FRP debonding are considered. The cracks occurring in the interface region from various loading conditions of FRP-retrofitted RC columns are of interest in this study. Also, FRP debonding as a result of imperfect strengthening construction may occur in real situations due to the air voids trapped between FRP and concrete during construction. Figure 7(b) shows a real FRP debonding situation in a bridge where an air void with approximately 3-cm diameter was discovered. As such, the proposed radar NDE aims at the detection of structural damages in the surface region of FRP-strengthened RC structures.

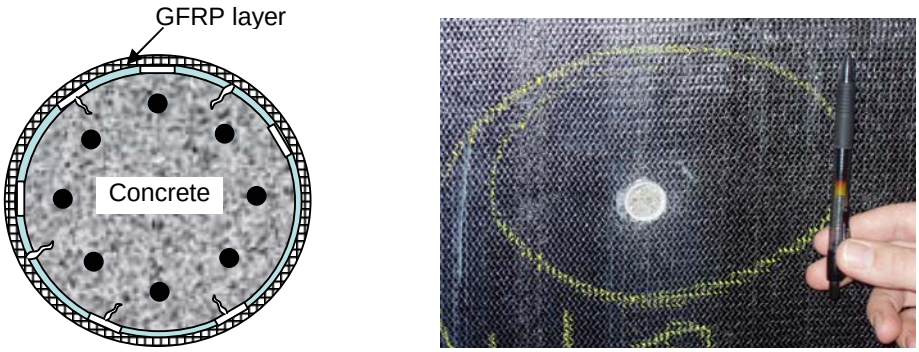

(a) Concrete cracking and FRP debonding

(b) Detected real GFRP debonding in a bridge

Figure 7 Structural damages and real FRP debonding.

Description of NDE Specimens with Simulated Damages

In the physical laboratory specimens artificial damages in GFRP-wrapped concrete cylinders are simulated by the introduction of single artificial anomaly (filled by air) between the GFRP layer and the surface region of concrete. Column reinforcements are not included in the physical concrete specimens. Due to our primary interest of detecting debonding and cracks in the interface region, the use of high-frequency, wide-bandwidth radar with penetration depth of up to 5 cm would allow the detection of interfacial cracks and voids with sufficient resolution.

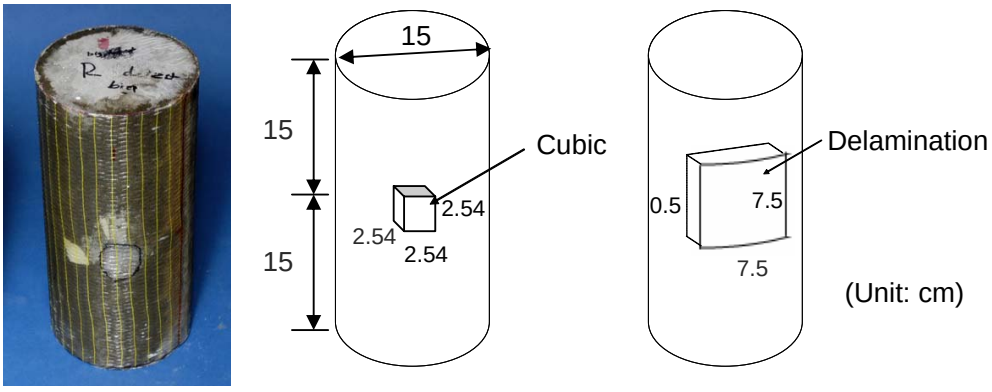

(a) CYLAD1 (b) CYLAD2

Figure 8 Two artificially damaged GFRP-concrete cylinder specimens.

Two artificially damaged GFRP-wrapped concrete cylinder specimens were prepared for physical radar measurements (Figure 8). Artificial damages were introduced by insertion of Styrofoam elements (whose dielectric properties are same as air) on the surface of concrete cylinders, representing construction defect (CYLAD1, Figure 8(a)) and GFRP debonding (CYLAD2, Figure 8(b)). The artificially damaged concrete specimens were then wrapped by GFRP sheet which adhered to the concrete with epoxy. The average 28-day strength of the concrete was 26MPa. The water-to-cement ratio was 0.6.

Physical Radar Measurement

The physical radar measurements of GFRP-confined concrete cylinder specimens were collected at MIT Lincoln Laboratory using the Compact Radar Cross Section (RCS)/Antenna Range facility. The experimental set-up consists of a horn antenna, stepped-frequency radar and network analyzer systems, and a Harris Dual-Shaped reflection system, Model 1606, designed for conducting far-field studies. The facility can achieve high signal-to-noise ratio measurements for a large frequency bandwidth ranging from UHF (0.7 GHz) to 100 GHz. This radar system is capable of producing a 20-*m* quiet zone, different antenna radiation patterns, and full polarimetric RCS measurements. Specimens are placed on top of a Styrofoam tower that is capable of fully rotating the target at predetermined angular steps. The measurements were conducted in stepped-frequency mode by sweeping from a starting frequency f_1 to an end frequency f_2 in 0.02 *GHz* increments at a fixed angle. The target is then rotated to the next angular step and the frequency sweeping is again performed.

Radar measurements were conducted at X- and Ku-band frequencies (8-12 and 12-18 GHz, respectively) to achieve optimized resolution and surface penetration capabilities. The total rotation angle is 60° in the ISAR measurements and angular increments are $0.1°$ and $0.2°$. Two types of polarizations were used in the radar measurements: HH-polarization and VV-polarization.

Measurement Schemes

For radar measurements, the specimens under investigation were placed on top of a Styrofoam tower in two alternative orientations: 1) having the specimen rest on one of its ends, referred to as vertical position, and 2) having the specimen rest on its side, referred to as horizontal position. Schematics of the two measurement schemes are presented in Figure 9. For the specimen with vertical orientation (Figure 9 (a)) the angle of incidence θ is at $90°$ with the z-axis, thus the corresponding radar measurements are always made at normal incidence as the specimen is rotated around its axis. In the oblique incidence scheme (Figure 9(b)), the angle of incidence ϕ varies as the specimen rotates around the y-axis. Normal incidence is encountered only when the direction of incident waves and the axis of the specimen are perpendicular to each other. For all other incidences, the incident wave meets the specimen in an oblique fashion. Both measurement schemes were designed to capture different EM wave scattering behaviors, and consequently investigate their effectiveness when the far-field radar technique is applied for damage or defect detection in GFRP-confined concrete elements.

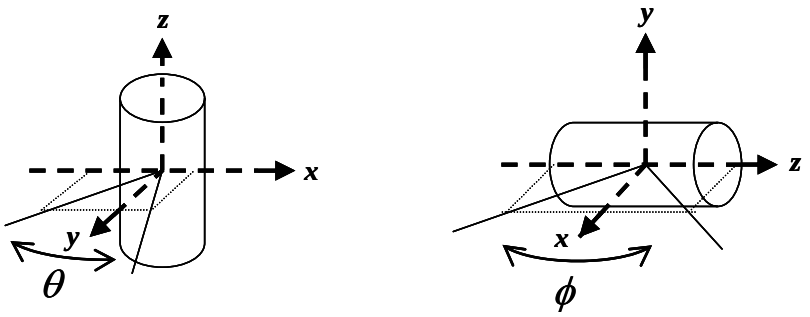

(a) Normal incidence (b) Oblique incidence

Figure 9 Normal incidence and oblique incidence measurement schemes.

Measurement Results

The radar measurements were collected in ISAR mode, and they consisted of HH and VV polarization measurements as functions of frequency at fixed incident angles. For each polarization, an amplitude entry and a phase entry were recorded at each frequency step. Measurement results are processed and rendered in frequency vs. angle imagery as shown in Figures 10~12. Only HH polarization (transverse electric or TE waves) measurements at X-band are reported. Figure 10 shows the far-field radar measurements in HH polarization at X-band from intact (without defect) and damaged (with defect) surfaces of the specimen CYLAD1 using normal incidence scheme. Figures 11 and 12 show the oblique incidence measurements from specimens CYLAD1 and CYLAD2, respectively.

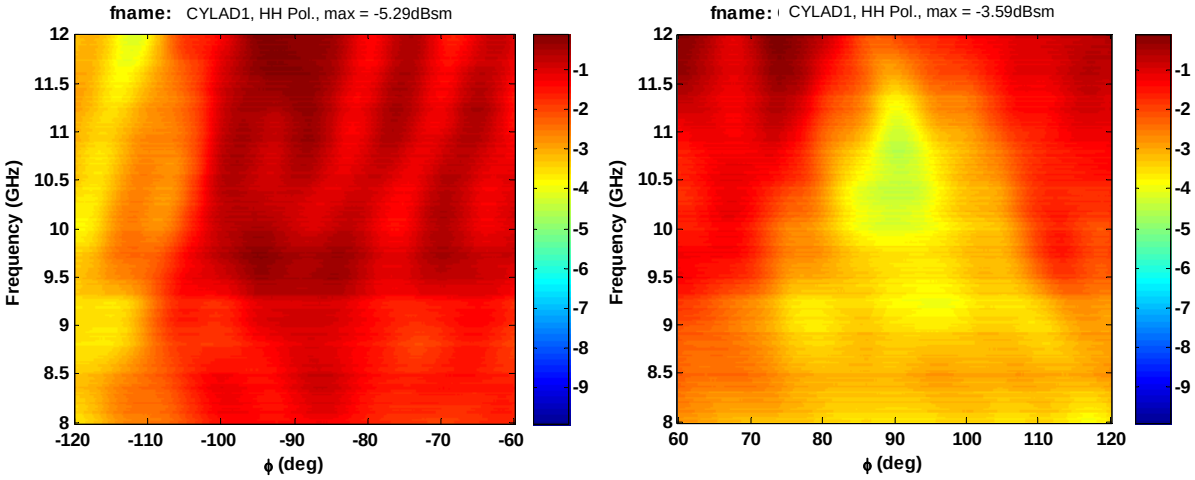

Figure 10 Frequency – angle imagery for specimen CYLAD1 measured at normal incidence, intact (left) and damaged (right) surfaces.

In Figure 10 it is observed that specular return dominates the reflection responses of intact and damaged cylinders in the normal incidence measurement scheme, although an area with relatively weak reflection is discovered in the position where the artificial defect is placed (85º~95º). This specular effect can be avoided by the use of oblique incidence measurement scheme (Figure 9(b)). The measurements taken in oblique incidence scheme clearly indicate the difference between intact and damaged cylinders. Such difference also depends on the characteristics of the defect, as shown in Figures 11

and 12. It is noteworthy to point out that specular return can still occur when incident angle equals 90º even in the oblique incidence measurement scheme. This is the normal reflection in oblique incidence measurements.

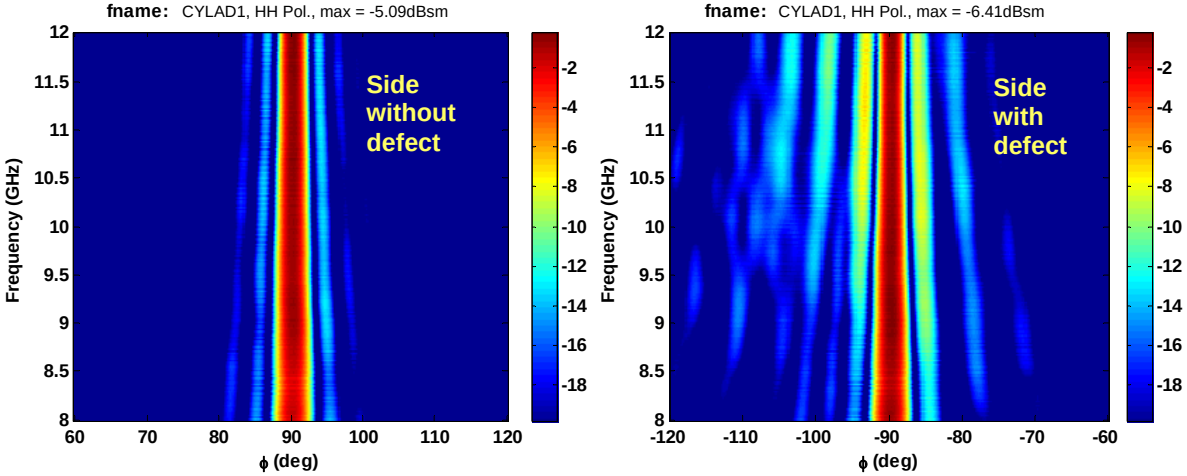

Figure 11 Frequency – angle imagery for specimen CYLAD1 measured at oblique incidence, intact (left) and damaged (right) surfaces.

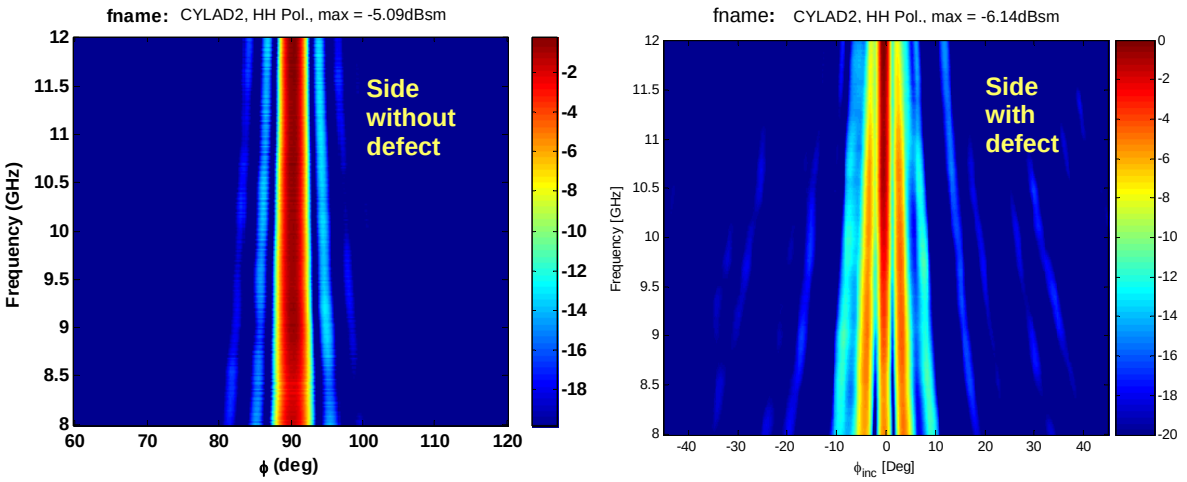

Figure 12 Frequency – angle imagery for specimen CYLAD2 measured at oblique incidence, intact (left) and damaged (right) surfaces.

Numerical Simulation

Radar signals or microwaves are all EM waves and their behaviors are governed by the laws of electricity and magnetism, or the Maxwell equations which regulate the relations and interactions between electric and magnetic fields. For the purpose of numerical implementation using difference equation, the curl form of Maxwell's equations is applied (Kong, 2000). The far-field EM wave propagation and scattering is modeled in numerical domain as a source-free problem in which no dipole moment source is considered inside the domain. The Maxwell curl equations are evaluated by the finite difference-time domain (FD-TD) method in both space and time. The FD-TD

method using Yee's algorithm (Yee, 1966) was implemented by a computer program written in Matlab (Matrix Laboratory) developed by the authors.

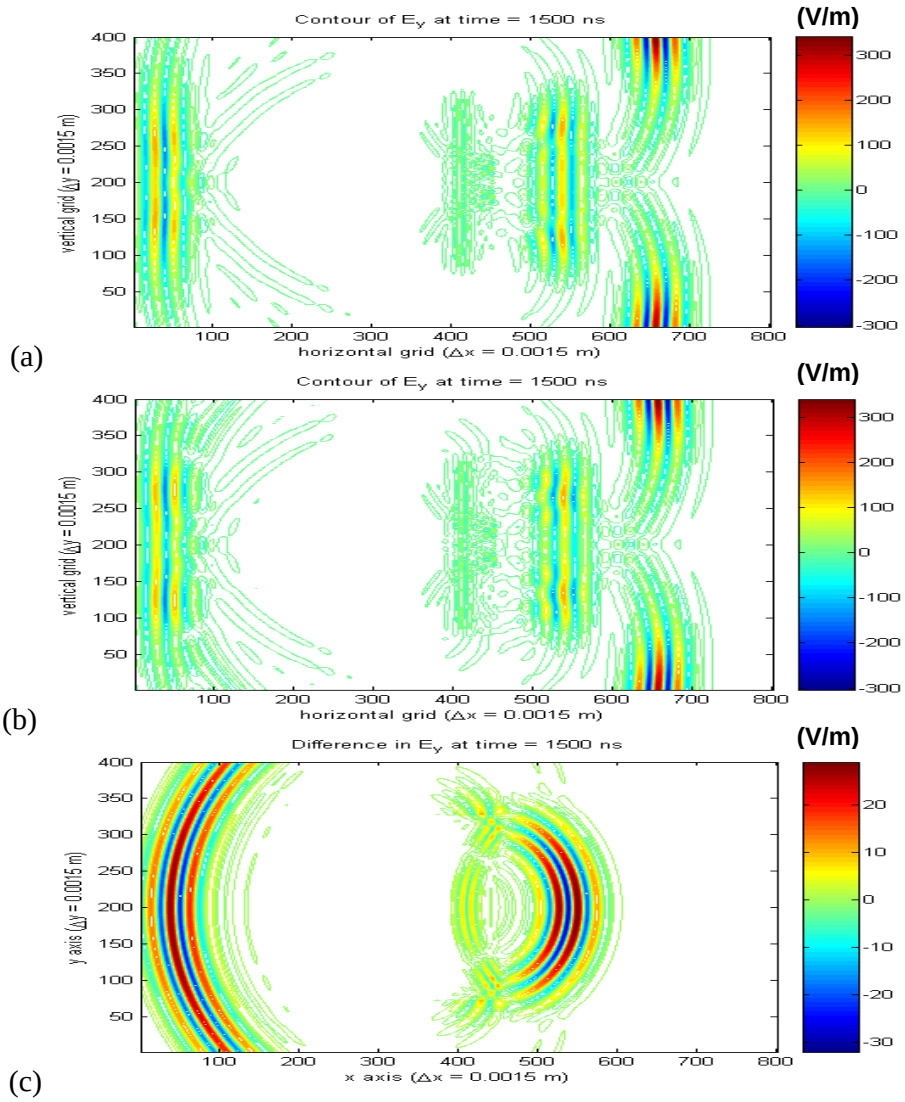

Figure 13 E_y fields of (a) intact, (b) damaged cylinders and (c) their difference.

Simulated EM wave propagation and scattering through the intact and damaged cylinders was generated in a numerical domain. TE waves were adopted, in which time- and space-dependent E_x, E_y, and H_z components of the waves are evaluated in the simulation. Intact and artificially damaged GFRP-wrapped concrete cylinders were subjected to the impinging of a modulated Gaussian transient signal with carrier frequency of 8GHz. In the simulation, dielectric constants and loss factors used are 5.69 and 0.62 for concrete, 4 and 0.001 for GFRP-epoxy, respectively (Büyüköztürk et al, 2006a). Simulated scattered E_y fields from intact and damaged cylinders, together with the difference between these fields, corresponding to the time of 1500ns are provided in Figure 13. The difference between the scattered fields obtained from the intact and damaged specimens relates to the artificial damage introduced in the specimen. Details of this numerical simulation can be found in Büyüköztürk and Yu (2006b).

Imaging Results

Image reconstruction using the fast backprojection algorithm by Yegulalp (1999) was performed on the physical radar measurements of CYLAD1 and CYLAD2, and intact GFRP-concrete cylinders. Figure 14 shows the imagery of intact cylinder at 75º and 90º in the oblique measurement scheme. The position of the cylinder is indicated in all images. It is observed that strong specular effect occurs when the direction of EM waves is perpendicular to the longitudinal axis of the cylinder, as shown in the 90º image. Such specular effect is decreased or avoided when the cylinder is placed at angles other than 90º (normal reflection), such as 75º. Figures 15 and 16 show the imagery of specimens CYLAD1 and CYLAD2 at the normal reflection and the angle 15º deviating from the normal reflection.

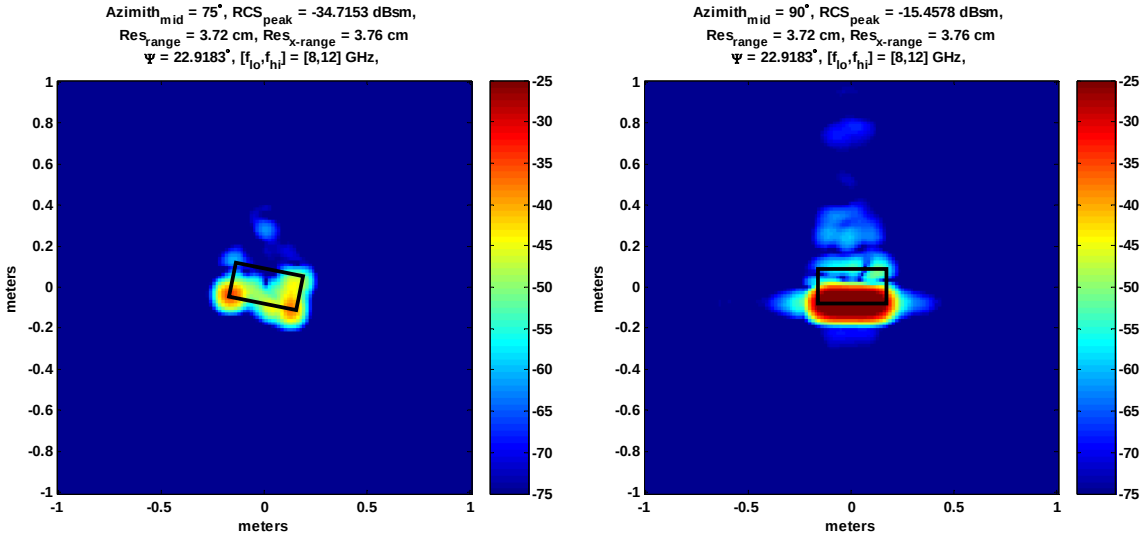

Figure 14 Range – cross-range imagery for intact specimen measured at oblique scheme, 75º (left) and 90º (right) surfaces.

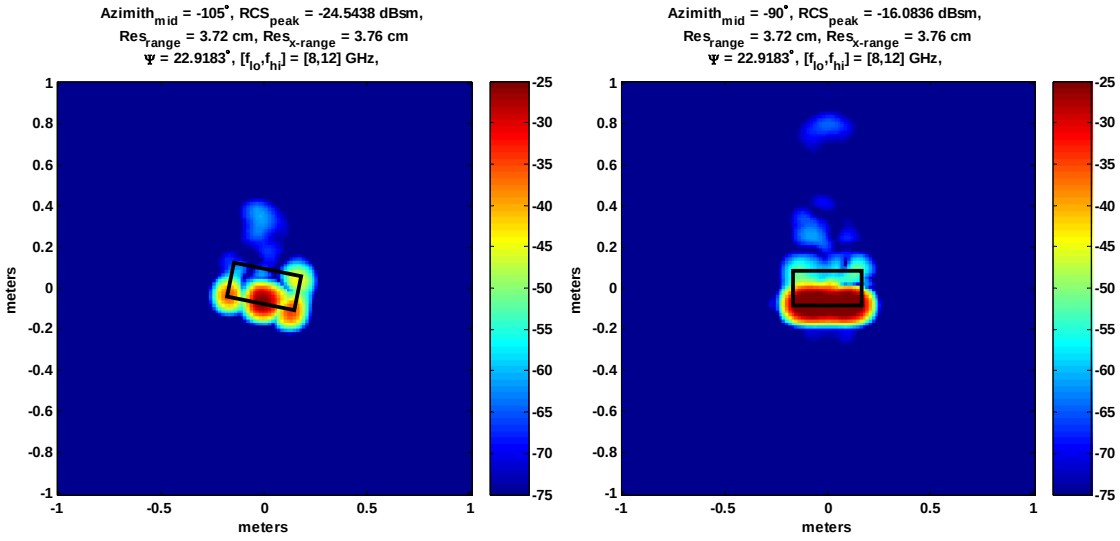

Fig. 15 Range – cross-range imagery for specimen CYLAD1 measured at oblique scheme, 75º (left) and 90º (right) surfaces.

From these imaging results, the capability of far-field airborne radar NDE technique on assessing the debonding failures in the surface region of GFRP-wrapped concrete cylinders is verified. Damage signatures appearing in the imagery are clearly identified for defects with thickness as small as 0.5cm and area as small as 2.54-by-2.54 cm^2.

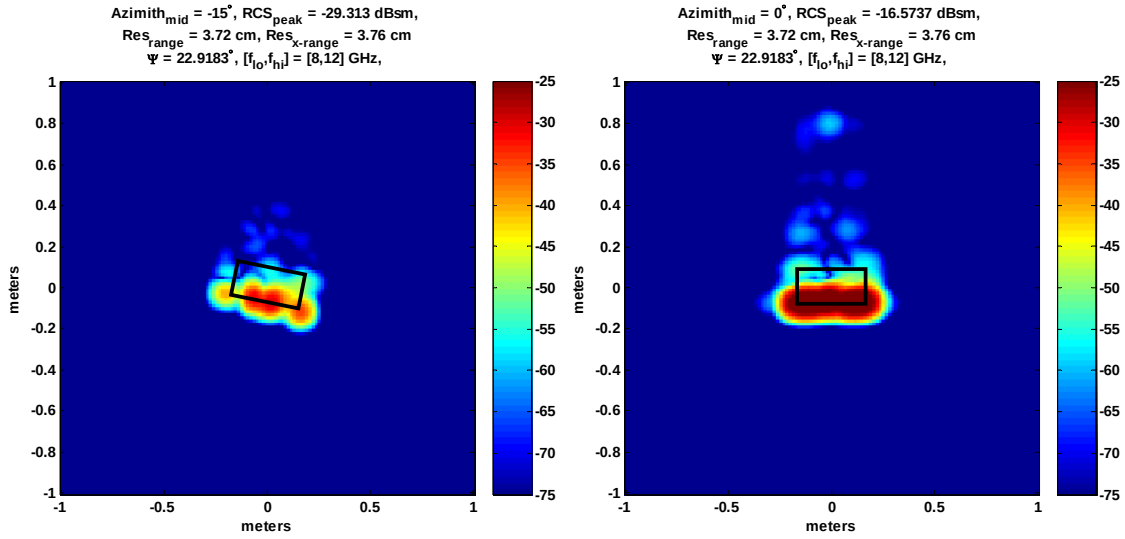

Fig. 16 Range – cross-range imagery for specimen CYLAD2 measured at oblique scheme, -15º (left) and 0º (right) surfaces.

Conclusion

Experimental evidences and modeling studies have shown that FRP debonding is a highly complex phenomenon that can involve failure propagation within the concrete substrate, within the adhesive, within the FRP laminate, and along the interfaces of these constituent materials. Effects of moisture and temperature may be significant on debonding involving physical changes in the interface region and leading to failure. This phenomenon can be characterized using the interface fracture toughness of the joint as a quantifying measure. Further research is needed for better understanding and quantification of environmental effects on debonding failures in FRP/adhesive/concrete systems.

A far-field airborne radar (FAR) NDE technique aiming at the damage detection in the surface region of GFRP-wrapped concrete structures is proposed. To validate the feasibility of the technique physical radar measurements and numerical simulations were performed. Physical radar measurements on GFRP-wrapped concrete cylinder specimens with artificially introduced air voids and delamination behind the GFRP layer were collected at X- and Ku-bands in a compact/radar cross section antenna facility. The radar antenna operated in inverse synthetic aperture radar (ISAR) mode providing reflection measurements at different angles. Two measurement schemes, normal incidence and oblique incidence, were investigated. Based on the findings from this stage of the research, it is believed that the surface damages (GFRP delamination, concrete cracking) on concrete behind the GFRP layer can be detected by the far-field radar measurements. Further work is underway for radar measurements and numerical

simulation of mechanically damaged specimens, and data de-noising and filtering for signal processing. Additional work is planned for ISAR imaging and interpretation of damage patterns.

Acknowledgement

Part of the work reported in this paper was supported by the National Science Foundation through Grants CMS-0324607 and CMS-0010126, and by the MIT Lincoln Laboratory through Grant ACC-376 (Advanced Concepts Committee). Data regarding the effects of moisture and temperature on FRP debonding was developed by Dr. C. Au as part of his PhD thesis under the supervision of the first author. Physical radar measurements were performed at MIT Lincoln Laboratory under the supervision of Dennis Blejer. The authors would like to acknowledge his efforts and contribution to the research reported in this paper.

References

Ahmad, O., D.V. Gemert, and L. Vadewalle (2001) Improved model for plate-end shear of CFRP strengthened RC beams, Cement and Concrete Composites, Vol. 23, pp.3-19.

Akuthota, B., D. Hughes, R. Zoughi, J. Myers, and A. Nanni (2004) Near-field microwave detection of disband in carbon fiber reinforced polymer composites used for strengthening cement-based structures and disband repair verification. Journal of Materials in Civil Engineering, Vol. 16, No. 6, pp.540-546.

Antoon, M.K., and J.L. Koenig (1980) The structure and moisture stability of the matrix phase in glass- reinforced epoxy composites. Journal Macromolecular Science – Reviews of Macromolecular Chemistry, Vol. C19, No. 1, pp.135-173.

Au, C. (2005) Moisture degradation in FRP bonded concrete systems: an interface fracture approach. PhD Thesis, Department of Civil and Environmental Engineering, Massachusetts Institute of Technology, Cambridge, MA.

Au, C., and O. Büyüköztürk (2006a) Peel and shear fracture characterization of debonding in FRP plated concrete affected by moisture. Journal of Composites for Construction, Vol. 10, No. 1, pp.35-47.

Au, C., and O. Büyüköztürk (2006b) Debonding of FRP plated concrete: a tri-layer fracture treatment. Engineering Fracture Mechanics, Vol. 73, pp.348-365.

Bastianini, F., A.D. Tommaso, and G. Pascale (2001) Ultrasonic non-destructive assessment of bonding defects in composite structural strengthenings. Composite Structures, Vol. 53, pp.463-467.

Berriman, J.R., D.A. Hutchins, A. Neild, T.H. Gan, and P. Purnell (2006) The application of time-frequency analysis to the air-coupled ultrasonic testing of concrete. IEEE Transaction on Ultrasonics, Ferroelectrics, and Frequency Control, Vol. 53, No. 4, pp.768-777.

Büyüköztürk, O. (1998) Imaging of concrete structures. NDT&E International, Vol. 31, No. 4, pp.233-243.

Büyüköztürk, O., B. Hearing, and O. Gunes (1999a) Performance and durability related issues in retrofitting concrete members with FRP. Proceedings of the 13th ASCE Engineering Mechanics Division Conference, June 13-16, The John Hopkins University, Baltimore, MD.

Büyüköztürk, O., B. Hearing, and O. Gunes (1999b) Failure of Concrete Beams Strengthened with Fiber Reinforced Plastic Laminates, Chapter 3, Mechanics of Quasi-Brittle Materials and Structures, edited by G.Pijaudier-Cabot, Z. Bazant, and B. Gerard, HERMES Science Publications, Paris, France.

Büyüköztürk, O., J. Park, and C. Au (2003) A novel approach to non-destructive evaluation of FRP-confined concrete using microwaves. Proceedings of International Symposium on Non-Destructive Testing in Civil Engineering, September 16-19, Berlin, Germany.

Büyüköztürk, O., O. Gunes, and E. Karaca (2004) Progress on understanding debonding problems in reinforced concrete and steel members strengthened using FRP composites. Construction and Building Materials, Vol. 18, pp.9-19.

Buyukozturk, O., T.-Y. Yu, and J.A. Ortega (2006a) A methodology for determing complex permittivity of construction materials based on transmission-only coherent, wide-bandwidth free-space measurements. Cement & Concrete Composites, Vol. 28, pp.349-359.

Büyüköztürk, O., and T.-Y. Yu (2006b) Detecting deterioration behind GFRP wrap strengthening of bridge columns. Proceedings of Structural Faults + Repair 2006, Edinburgh, UK.

Chajes, M.J., T.A. Thompson, and C.A. Farschman (1995) Durability of concrete beams externally reinforced with composite fabrics. Construction & Building Materials, Vol. 9, no. 3, pp.141-148.

Chen, H.-L. R., and Y. He (2001) Analysis of acoustic surface waveguide for AE monitoring of concrete beams. Journal of Engineering Mechanics, Vol. 127, No. 1, pp.1-10.

Clark, M.R., D.M. McCann, and M.C. Forde (2003) Application of infrared thermography to the non-destructive testing of concrete and masonry bridges. NDT & E International, Vol. 36, pp.265-275.

Collotti, V., and G. Spadea (2001) Shear strength of RC beams strengthened with bonded steel or FRP plates. Journal of Structural Engineering, Vol. 127, No. 4, pp.367-373.

Daigle, M., D. Fratta, and L.B. Wang (2005) Ultrasonic and X-ray tomographic imaging of highly contrasting inclusions in concrete specimens. Proceedings of Site Characterization and Modeling (GSP-138), P.W. Mayne, E. Rathje, J. DeJong, A. Rechenmacher, J. Yamamuro, S. Sharma, and C. Willson (ed.), January 24–26, Austin, TX.

Di Tommaso, A., U. Neubauer, A. Pantuso, and F.S. Rostasy (2001) Behavior of adhesively bonded concrete-CFRP joints at low and high temperatures. Mechanics of Composite Materials, Vol. 37, No. 4, pp.327-338.

El-Mihilmy, M.T., and J.W. Tedesco (2001) Prediction of anchorage failure for reinforced concrete beams strengthened with fiber-reinforced polymer plates. ACI Structural Journal, Vol. 98, No. 3, pp.301-314.

Feng, M.Q., F.D. Flaviis, and Y.J. Kim (2002) Use of microwaves for damage detection of fiber reinforced polymer-wrapped concrete structures. Journal of Engineering Mechanics, Vol. 128, No. 2, pp.172-183.

Fukuzawa, K., T. Numao, Z. Wu, H. Yoshizawa, and M. Mitsui (1997) Critical strain energy release rate of interface debonding between carbon fiber sheet and mortar. Proceedings of the 3rd International Symposium of Non-Metallic (FRP) Reinforcement for Concrete Structures, Japan, pp.295-302.

Green, M.F., L.A. Bisby, Y. Beaudoin, and P. Labossiere (2000) Effect of freeze-thaw cycles on the bond durability between fibre reinforced polymer plate reinforcement and concrete. Canadian Journal of Civil Engineering, Vol. 27, No. 5, pp.949-959.

Gunes, O. (2004) A fracture-based approach to understanding debonding in FRP bonded structural members. PhD Thesis, Department of Civil and Environmental Engineering, Massachusetts Institute of Technology, Cambridge, MA.

Hamilton, H.R.III (2000) Durability of FRP reinforcements for concrete. Progress in Structural Engineering and Materials, Vol. 2, pp.139-145.

Hamoush, S.A., and S.H. Ahmad (1990) Debonding of steel plate-strengthened concrete beams. Journal of Structural Engineering, Vol. 116, No. 2, pp.356-371.

Hag-Elasfi, O., S. Alampalli, and J. Kunin (2004) In-service evaluation of a reinforced concrete T-beam bridge FRP strengthening system. Composite Structures, Vol. 64, pp.179-188.

Hutchinson, A.R. (1986) Durability of structural adhesive joints. Ph.D. Thesis, Dundee University, UK.

Karbhari, V.M., and M. Engineer (1996) Investigation of bond between concrete and composites. Journal of Reinforced Plastics and Composites, Vol. 15, No. 2, pp.208-227.

Karbhari, V.M., and L. Zhao (1998) Issues related to composite plating and environmental exposure effects on composite-concrete interface in external strengthening. Composite Structures, Vol. 40, No. 3-4, pp.293-304.

Kinloch, A.J. (1982) The science of adhesion. Journal of Materials Science, Vol. 17, No. 3, pp.617-651.

Kong, J.A. (2000) Electromagnetic Wave Theory, EMW Publishing, Cambridge, MA.

Lau, K.T., S.Q. Shi, and L.M. Zhou (2001) Estimation of stress intensity factor (KI) for an FRP bonded beam using the superposition method. Magazine of Concrete Research, Vol. 53, No. 1, pp.31-41.

Leung, C.K.Y. (2001) Delamination failure in concrete beams retrofitted with a bonded plate. Journal of Materials in Civil Engineering, Vol. 13, No. 2, pp.106-113.

Li, J., and C. Liu (2001) Noncontact detection of air voids under glass epoxy jackets using a microwave system. Subsurface Sensing Technologies and Applications, Vol. 2, No. 4, pp. 411-423.

Malek, A.M., H. Saadatmanesh, M.R. Ehsani (1998) Prediction of failure load of R/C beams strengthened with FRP plate due to stress concentration at plate end. ACI Structural Journal, Vol. 95, No. 2, pp.142-152.

Mirmiran, A., and S. Philip (2000) Comparison of acoustic emission activity in steel-reinforced and FRP-reinforced concrete beams. Construction and Building Materials, Vol. 14, pp.299-310.

Mirmiran, A., and Y. Wei (2001) Damage assessment of FRP-encased concrete using ultrasonic pulse velocity. Journal Engineering Mechanics, Vol. 127, No. 2, pp.126-135.

Oehlers, D.J. (1992) Reinforced concrete beams with plates glued to their soffits. Journal of Structural Engineering, Vol. 118, No. 8, pp.2023-2038.

Quantrill, R.J., L.C. Hollaway, and A.M. Throne (1996) Predictions of the maximum plate end stresses of FRP strengthened beams: part II. Magazine of Concrete Research, Vol. 48, No. 177, pp.343-351.

Owen, R.D. (1998) Portable linear accelerators for X-ray and electro-beam applications in civil engineering. NDT&E International, Vol. 31, No. 6, pp.401-409.

Popovics, J.S., and J.L. Rose (1994) Survey of developments in ultrasonic NDE of concrete. IEEE Transactions on Ultrasonics, Ferroelectrics, and Frequency Control, Vol. 41, No. 1, pp.140-143.

Rabinovitch, O., and Y. Frostig (2001) Delamination failure of RC beams strengthened with FRP strips – a closed-form high-order and fracture mechanics approach. Journal of Engineering Mechanics, Vol. 127, No. 8, pp.852-861.

Roberts, T.M. (1989) Approximate analysis of shear and normal stress concentrations in the adhesive layer of plated RC beams. The Structural Engineer, Vol. 67, No. 12, pp.229-233.

Roberts, T.M., and H. Haji-Kazemi (1989) A theoretical study of the behavior of reinforced concrete beams strengthened by externally bonded steel plates. Proceedings of Institution of Civil Engineers – Part 2, Vol. 87, pp.39-55.

Smith, S.T. and J.G. Teng (2001) Interfacial stresses in plated beams. Engineering Structures, Vol. 23, No. 7, pp.857-871.

Smith, S.T., and J.G. Teng (2002) FRP-strengthened RC beams II: assessment of debonding strength models. Engineering Structures, Vol. 24, No. 4, pp.397-417.

Starnes, M.A., N.J. Carino, and E. Kausel (2003) Preliminary thermography studied for quality control of concrete structures strengthened with fiber-reinforce polymer composites. Journal of Materials in Civil Engineering, Vol. 15, No. 3, pp.266-273.

Swit, G. (2004) Evaluation of compliance changes in concrete beams reinforced by glass fiber reinforced plastics using acoustic emission. Journal of Materials in Civil Engineering, Vol. 16, No. 5, pp.414-418.

Tanigawa, Y., K. Yamada, and S. Kiriyama (1997) Frequency characteristics of AE in concrete. Proceedings of Japan Concrete Institute, Vol. 2, pp.129-132.

Teng, J.G. (2006) Debonding failures of RC beams flexurally strengthened with externally bonded FRP reinforcement. Proceedings of Structural Faults + Repair 2006, Edinburgh, UK.

Toutanji, H., and W. Gomez (1997) Durability characteristics of concrete beams externally bonded with FRP composite sheets. Cement and Concrete Composites, Vol. 19, No. 4, pp.351-358.

Varastehpour, H., and P. Hamelin (1997) Strengthening of concrete beams using fiber-reinforced plastics. Material Structures, Vol. 30, pp.160-166.

Yee, K.S. (1966) Numerical solution of initial boundary value problems involving Maxwell's equations in isotropic media", IEEE Transactions on Antennas and Propagation, Vol. AP-14, No. 3, pp.302-307.

Yegulalp, A.F. (1999) Fast backprojection algorithm for synthetic aperture radar. The Record of the 1999 IEEE Radar Conference, pp.60-65.

Ziraba, Y.N., M.H. Baluch, I.A. Basunbul, A.M. Sharif, A.K.Azad, and G.J Al-Sulaimani (1994) Guidelines toward the design of reinforced concrete beams with external plates. ACI Structural Journal, Vol. 91, No. 6, pp.639-646.